J. Fluid Mech. (1988), *vol.* 191, *pp.* 557–573
Printed in Great Britain

Cylindrical solitary waves

By P. D. WEIDMAN AND R. ZAKHEM
Department of Mechanical Engineering, University of Colorado, Boulder, CO 80309, USA

(Received 19 August 1981 and in revised form 4 November 1987)

Experiments on the radial propagation of axisymmetric free-surface solitary waves are reported and compared with theoretical and numerical solutions of the cylindrical Korteweg–de Vries (CKdV) equation. A new experimental technique to obtain a continuous amplitude signature on photographic paper is reported. These measurements show that an isolated disturbance evolves into a slowly varying solitary wave with amplitude decaying as $r^{-\frac{2}{3}}$, where r is the radius measured from the centre of the disturbance. A numerical study of the CKdV equation is made to interpret the transient development of these waves into the nonlinear asymptotic regime. It is further pointed out that the CKdV equation also describes weakly nonlinear axisymmetric internal waves, and a comparison of theory for this case with internal-wave trajectory measurements reported by Maxworthy (1980) exhibit good agreement.

1. Introduction

When the effects of geometrical distortion on a propagating gravity wave are comparable with those of amplitude nonlinearity and phase dispersion, it is not uncommon to find that its mathematical description can be reduced to some form of a variable-coefficient Korteweg–de Vries (KdV) equation. Kakutani (1971) and Johnson (1973), for example, have derived variable-coefficient KdV equations describing the effect of changing fluid depth on long, one-dimensional shallow-water waves. Shuto (1974), Ostrovoskiy & Pelinovskiy (1975), and Miles (1977) have each derived such equations to account for variable channel cross-section. With an interest in radially propagating ion-acoustic waves, Maxon & Viecelli (1974) introduced and analysed what will hereinafter be called the cylindrical Korteweg–de Vries (CKdV) equation. Their numerical results demonstrated that inward-propagating cylindrical waves may be characterized as slowly varying solitary waves in that $a\lambda^2 = \text{const.}$, where a is the wave amplitude and λ its wavelength. Using similarity arguments and energy conservation, Cumberbatch (1978) further interpreted the numerical results of Maxon & Viecelli (1974), showing that the amplitude dependence on radial position is given by $a \propto r^{-\frac{2}{3}}$, where r is the radial coordinate from the origin of the disturbance. This nonlinear Green's law was actually derived earlier by Miles (1977) in the context of nonlinear waves propagating in channels with slowly converging or diverging sidewalls.

Solutions for variable-coefficient KdV equations have been reported by a number of authors. Leibovich & Randall (1973) may be credited as the first to discover (via their numerical work) the existence of a 'shelf', a flat wave of elevation or depression which evolves behind slowly varying solitary waves, and later Kaup & Newell (1978) predicted them analytically using inverse scattering methods. Miles (1978) was the first to derive the CKdV equation in the context of free-surface gravity waves and

considered in detail similarity solutions for both dispersive and solitary waves. Ko & Kuehl (1978, 1979) have also explicitly studied solitary waves governed by the CKdV equation as a particular case of their move general (albeit non-uniform) perturbation solution. Grimshaw (1979) extended the work of Ko & Kuehl by considering waves which depend on both slow time and slow space variables, and attempted to remove non-uniformities by matching to an outer expansion. Exact solutions to the CKdV equation are indeed difficult to find, but sec Calogero & Desgasperis (1978) and Grimshaw (1979).

Although in a different parameter regime, that of the self-focusing of nonlinear cylindrical waves, we mention the study of Chwang & Wu (1976) for completeness. One particularly interesting result of their numerical study was the observation of a phase shift between a radially inward-propagating wave and the outward-propagating wave formed by self-reflection in a constant-depth fluid. This represents the axisymmetric counterpart of the phase shift incurred by the *weak* interaction (head-on collision) of two planar solitions (see, for example, Su & Mirie 1980).

Experiments on solitary free-surface gravity waves in channels of variable cross-section are included in papers by Perroud (1957), Chang, Melville & Miles (1979), and Maxworthy (1980). Chang *et al.* and Perroud measured wave amplification (attenuation) in constant-depth channels with uniformly decreasing (increasing) breadth b at converging (diverging) angles of approximately 0.02 rad (0.1 rad). Miles (1977) found 'fairly satisfactory' agreement when comparing Perroud's data for the converging channel with the nonlinear Green's law, $a \propto b^{-\frac{2}{3}}$, but reported unsatisfactory agreement for the diverging channel. Chang *et al.* report good agreement between their measured and computed amplitudes for both converging and diverging channels when the effects of viscous damping are taken into account, and their measured wave profiles show evidence of the formation of shelf waves.

The results presented here provide further documentation of the nonlinear–dispersive balance for radially propagating cylindrical waves. In §2 we give a short derivation of the salient features of slowly varying axisymmetric solitary waves and mention their relevance to internal as well as free-surface waves. Measurements of the amplitude decay for outward-propagating free-surface waves are presented in §3 along with a comparison of theoretically predicted phase trajectories with internal-wave measurements reported by Maxworthy (1980). In order to better interpret the free-surface amplitude experiments, we include in §4 a short numerical study to investigate the influence of disturbance wave shape and wave volume on amplitude evolution as described by the CKdV equation. The discussion of results is presented in §5 and concluding remarks are given in §6.

2. Solution-like properties of the CKdV equation

We begin with the dimensional evolution equation for the free-surface displacement η of axisymmetric waves in a homogeneous fluid derived by Miles (1978)†

$$\frac{1}{c}\eta_t+\eta_r+\frac{\eta}{2r}+\frac{3}{2h}\eta\eta_r+\frac{1}{6}h^2\eta_{rrr}=0, \tag{1}$$

† This equation only describes unidirectional radially propagating waves and does not conserve mass. Hence it may only represent the asymptotic part of a true initial-value problem. Further discussion of this aspect of the problem is given by Miles (1978) and Chang *et al.* (1979).

where r, t, and h are respectively the radius, time, and quiescent fluid depth. Here $c = (gh)^{\frac{1}{2}}$ is the one-dimensional linear long-wave speed, with g the gravitational constant. The inherent balance between nonlinearity, dispersion, and radial spreading in (1) is ensured if $r = O(h^{\frac{5}{2}}/a^{\frac{3}{2}})$. A non-dimensional form suitable for numerical computation is given by

$$\zeta_\xi + \frac{\zeta}{2\xi} + \tfrac{3}{2}\zeta\zeta_\tau + \tfrac{1}{6}\zeta_{\tau\tau\tau} = 0, \tag{2}$$

where we have retained only the highest-order terms after applying the transformation

$$\xi = \epsilon^{\frac{3}{2}}\left(\frac{r}{h}\right), \quad \tau = \epsilon^{\frac{1}{2}}\left(\frac{r}{h} - \frac{ct}{h}\right), \quad \zeta = \frac{\eta}{\epsilon h},$$

under the assumption that the amplitude parameter $\epsilon = a/h$ is small. A final reduction to the variable-coefficient KdV equation

$$u_\xi + \frac{3}{2\xi^{\frac{1}{2}}}uu_\tau + \frac{1}{6}u_{\tau\tau\tau} = 0 \tag{3}$$

is furnished by the dependent-variable transformation $\zeta = u/\xi^{\frac{1}{2}}$. For future reference, we note that the equation describing dispersionless linear disturbances is obtained by neglecting the last two terms in (2). Solution of this truncated equation furnishes the linear decay law $a \propto r^{-\frac{1}{2}}$.

We first consider some simple results derived by viewing (2) as a constant-coefficient KdV equation forced by the radial distortion term $\zeta/2\xi$. In the absence of this term, the solution of (2) that decays to zero at both upstream and downstream infinity is given by

$$\zeta(\xi, \tau) = \alpha^2 \operatorname{sech}^2[\sqrt{3\tfrac{1}{2}}\alpha(\tau - \tfrac{1}{2}\alpha^2\xi)] \tag{4}$$

and we now allow the solition parameter α to be a slowly varying function of the distortion variable ξ. Multiplying (2) by ζ and integrating on τ for fixed ξ gives

$$\int_{-\infty}^{\infty} \zeta\zeta_\xi \, d\tau = -\frac{1}{2\xi}\int_{-\infty}^{\infty} \zeta^2 \, d\tau.$$

Calculating ζ_ξ with the aid of (4) and performing the quadratures yields the differential equation $\alpha_\xi = -\alpha/3\xi$, which has solution $\alpha = \text{const}\ \xi^{-\frac{1}{3}}$. In dimensional variables this gives the amplitude decay law

$$a = k_1 r^{-\frac{2}{3}}, \tag{5}$$

and the corresponding wave trajectory obtained by setting the phase in (4) equal to zero takes the form

$$t = \frac{1}{c}(r - k_2 r^{\frac{1}{3}}), \tag{6}$$

where k_1 and k_2 are constants.

These simple results can be compared with the perturbation solution of the variable-coefficient equation (3) reported by Ko & Kuehl (1978). Their results written in physical variables provides a description for the wave amplitude

$$\frac{a}{a_0} = \frac{1}{\gamma^{\frac{2}{3}}}[1 + k(1 - \tfrac{1}{3}\ln\gamma)], \tag{7}$$

the wave trajectory

$$t-t_0 = \frac{r_0}{c}\left[\gamma - \frac{3a_0}{2h}\left\{\gamma^{\frac{1}{3}} - 1 + \frac{k}{3}\gamma^{\frac{1}{3}}\ln\gamma\right\}\right], \tag{8}$$

and the nonlinear wave velocity

$$v = c\left[1 - \frac{a_0}{2h}\gamma^{\frac{2}{3}}\{1 - k(1-\tfrac{1}{3}\ln\gamma)\}\right]^{-1}, \tag{9}$$

where $\gamma = r/r_0$ and

$$k = \frac{2}{3\sqrt{3}}\left[\frac{a_0}{h}\right]^{-\frac{3}{2}}\left[\frac{r_0}{h}\right]^{-1}.$$

Equations (7)–(9) are valid as long as the radial distortion is sufficiently weak and the fractional energy loss $E = -(\frac{1}{3}k)\ln\gamma$ is small. The zero subscripts refer to initial reference values in the slowly varying regime where amplitude nonlinearity, phase dispersion, and radial distortion are of equal order. Note that our results for wave amplitude (5) and phase trajectory (6) give the correct first-order behaviours for (7) and (8), respectively.

Detailed features of wave evolution from an initial sech-squared disturbance centred at $\xi = 10$ are displayed in figure 1. The wave profiles have been obtained by numerical integration of (2) using periodic boundary conditions and following the finite-difference scheme used by Ko (1978). The numerical technique (Vliegenthart 1971) is $O(\Delta\tau^2)$ in ζ, ζ_τ, $\zeta_{\tau\tau\tau}$ and is $O(\Delta\xi^2)$ in ζ_ξ. This produces numerical errors $O(\Delta\xi^3)$ and $O(\Delta\tau^2\Delta\xi)$ in (2). The stability analysis for $\Delta\tau \ll 1$ imposes the constraint

$$\frac{\Delta\xi}{\Delta\tau^3} < 1.5,$$

which gives a limiting error $O(\Delta\tau^5)$. For the calculations presented here, $\Delta\tau$ was typically 0.2.

Since τ is the non-dimensional coordinate moving with the one-dimensional linear phase speed, displacements from $\tau = 0$ are due to a combination of nonlinear, dispersive, and radial distortion effects. In figure 1 a depression wave or 'shelf' of increasing width and decreasing depth is seen to form behind the primary disturbance, and is itself trailed by a weak dispersive tail. Calculated values of the peak amplitude ζ_p and maximum shelf height $|\zeta_s|$ (magnified by a factor of ten) are plotted versus the non-dimensional radius ξ in figure 2. In less than 10 radial units the primary disturbance has evolved into the $-\frac{2}{3}$-power amplitude decay law. The shelf, however, develops more slowly and does not attain its $-\frac{1}{2}$-power amplitude attenuation until the wave has propagated 30 radial units. Although the perturbation solution of Ko & Kuehl (1978) is strictly valid only near the wave crest, an evaluation of their theory far behind the crest does indicate the presence of a constant-amplitude shelf, but with a $-\frac{2}{3}$-power-law decay rate (cf. Ko & Kuehl 1979, equation (17)). The $-\frac{1}{2}$-power-law dependence, to be expected from a consideration of the shelf wave as a linear disturbance, is implicit in the work of Miles (1978) and is given explicitly in Chang *et al.* (1979, equation (1.7)) for the case of a channel with linearly varying breadth.

The CKdV equation also describes, not surprisingly, the evolution of cylindrically propagating internal waves in a stably stratified fluid. Following the analysis of

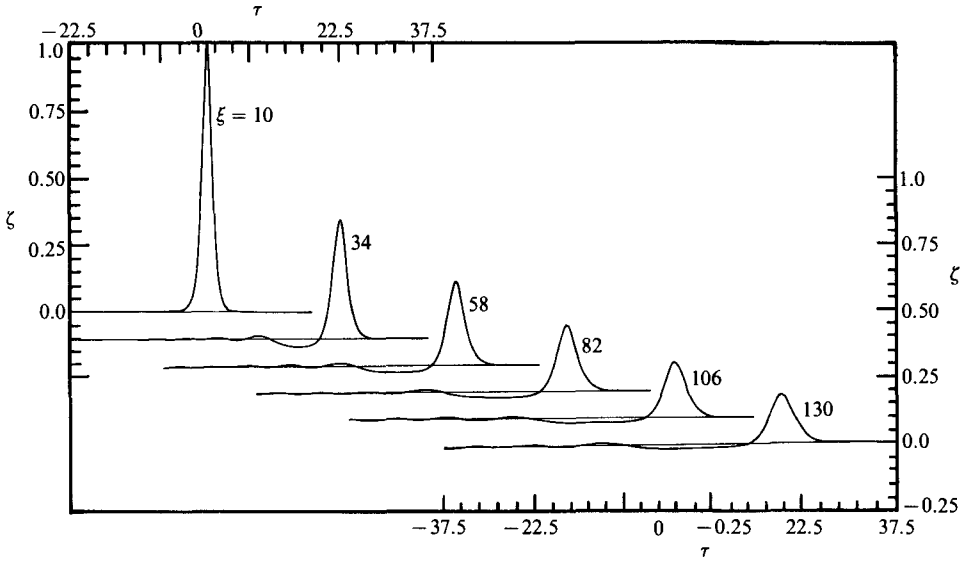

FIGURE 1. Profiles of axisymmetric wave evolution from an initial sech-squared disturbance centred at $\xi = 10$ obtained from numerical integration of the CKdV equation (2). Note the formation of a shelf of depression immediately following the solitary wave.

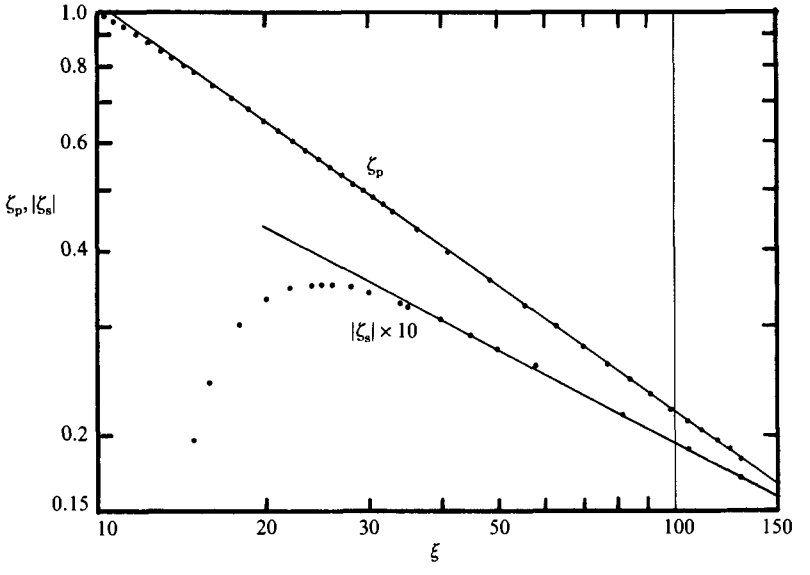

FIGURE 2. Peak amplitude decay of the primary wave ζ_p and formation of the trailing depression shelf with maximum amplitude $|\zeta_s|$. The points are numerical results and the solid curves correspond to $-\frac{2}{3}$- and $-\frac{1}{2}$-power-law decay rates.

Benney (1966), one can consider axisymmetric wave propagation in a stratified fluid bounded above and below by horizontal rigid walls to obtain the CKdV counterpart of Benny's KdV equation (76) with the same modal coefficients given by his equations (80) and (81). For the simplest case of a two-layer system with lower and upper fluid depths h_1, h_2 and densities ρ_1, ρ_2, respectively, only a single mode persists

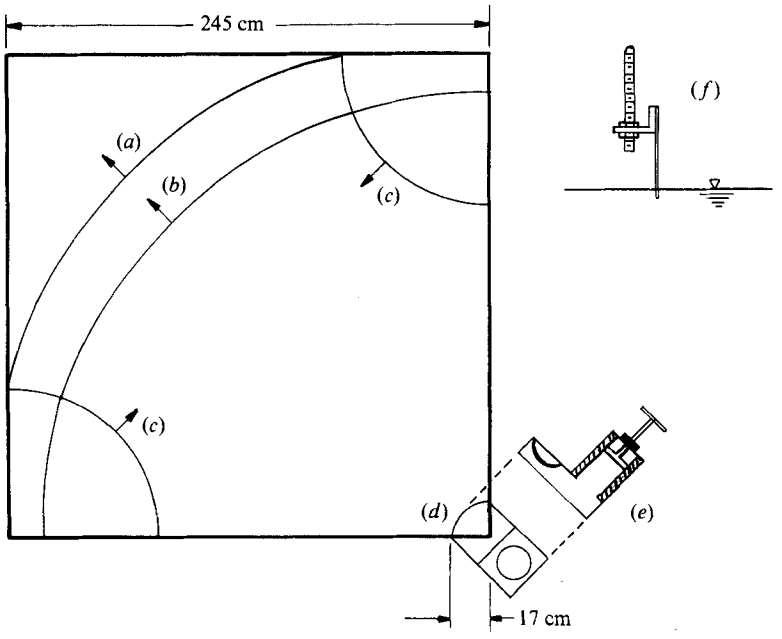

FIGURE 3. Diagram of the experimental facility showing the square tank and (*a*) the lead cylindrical wave, (*b*) the secondary cylindrical wave, (*c*) the reflected waves, (*d*) the quarter-circle diaphram, (*e*) the wave generator with piston near the top of its stroke, and (*f*) a detail of the photographic-paper suspension system.

and results (7), (8), and (9) remain valid if one replaces c by c_1, h by h_1, and redefine the linear wave speed c_1 as

$$c_1^2 = gh_1\left[\frac{(1-\sigma)(1-R)}{1-R(1-\sigma)}\right]. \tag{10}$$

Here $R = h_1/h$, $\sigma = \rho_2/\rho_1$, and $h = h_1 + h_2$ is the total fluid depth. This result for a two-layer fluid provides the basis for comparison of theory and experiment in §3.2.

3. Experimental procedure and results

All measurements were conducted in the square tank facility (245 cm on a side) previously used by Maxworthy (1980). Local disturbances initiated in one corner of the tank were observed to evolve into axisymmetric waves propagating outward across the 90° sector as shown in figure 3. It will soon be evident that free-surface waves easily lend themselves to amplitude but not trajectory measurement, while the opposite holds true for internal waves. Experimental measurements and comparison with theory for the free-surface and internal-wave systems are presented in the following two sections.

3.1. *Free surface cylindrical waves*

A hand-actuated piston (figure 3, detail (*e*)) provided the initial disturbance for the free-surface waves. This method of wave generation is similar to that employed by Hammack & Segur (1974) in that a volume of fluid is locally elevated at floor level. In the present case, however, the movable section in contact with the fluid was a flexible diaphragm in the shape of a quarter circle, rather than the rigid block used

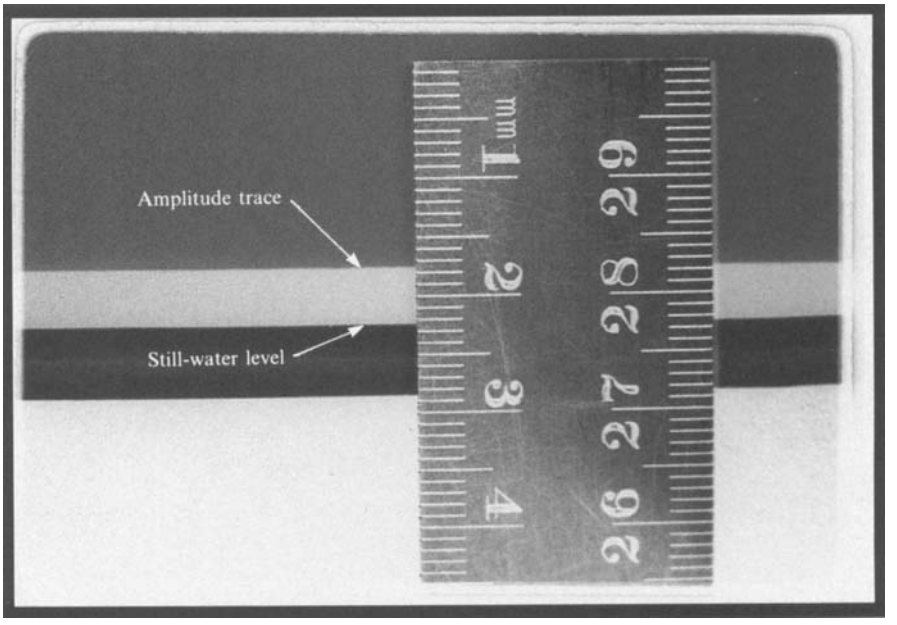

FIGURE 4. A short section of the exposed photographic strip exhibiting the still-water level and the peak-amplitude trace. The direction of wave propagation is from left to right.

by Hammack & Segur. The cavity between piston and diaphragm was filled with water such that at mid-stroke the diaphragm was level with the floor bottom; thus at the beginning (top) of the stroke the diaphragm expanded down below floor level, and at the completion (bottom) of the stroke it distended above. In all experiments reported here the displaced fluid volume was approximately 2100 cc and it will be assumed that the disturbance originated from the centroid of the diaphragm, located approximately 10 cm from the corner of the tank along its bisector. The speed of piston displacement allowed some qualitative control on the shape of the disturbance waveform as determined by light reflection off the wave crest; slow speeds produced long-wavelength disturbances of low amplitude, while fast speeds produced relatively shorter-wavelength, higher-amplitude waveforms.

Radial attenuation of the maximum wave height was measured by a novel, simple, yet surprisingly accurate measurement technique. The working fluid consisted of a solution of 20 parts water mixed with 1 part Kodak Flowmatic Fixer and the measuring device was unexposed photographic paper. Each experiment was performed under 'safe' lighting in the following manner. A long narrow strip of photosensitive paper was neatly cut and suspended vertically from a straight aluminium angle (figure 3, detail (*f*)). The angle was in turn suspended from a wooden beam spanning the top of the tank and resting in fixed blocks at diagonally opposite corners in line with and bisecting the submerged diaphram. At the beginning of a run, the piston was raised to the top of its stroke and the paper was gently immersed on edge 0.5 cm below the free surface, thus 'fixing' a line on the paper marking the undisturbed water level. Then the piston was manually actuated and the propagating wave wiped an elevated trace along the paper during its travel across the tank, thus 'fixing' the maximum amplitude signature. The support beam was removed from the liquid bath at an appropriate time before waves reflecting from the sidewalls (figure 3, detail (*c*)) impinged on the sensing surface of the paper

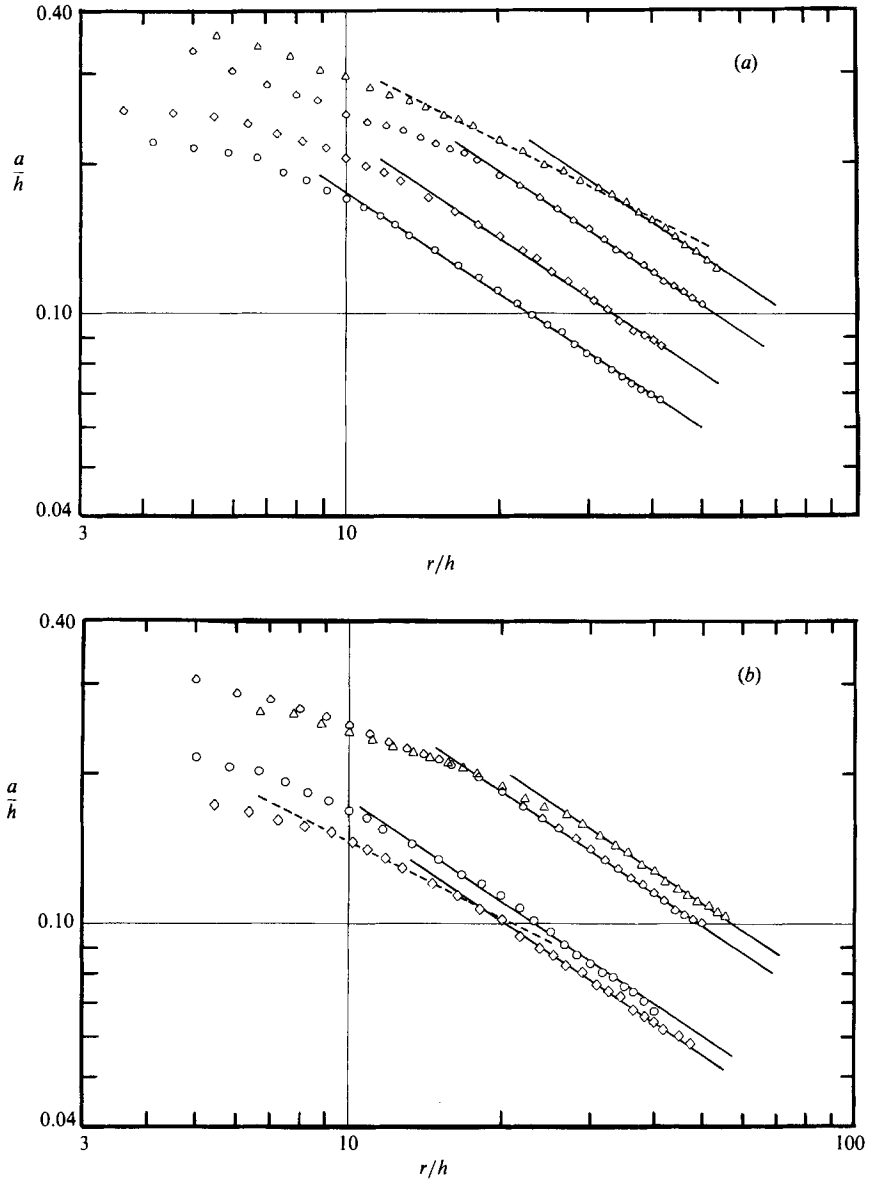

FIGURE 5. (*a*, *b*). Measured amplitudes from two sets of experiments for free-surface cylindrical waves propagating on quiescent fluid depths $h = 4.5$ cm (△), 5.0 cm (◇), 5.5 cm (◇), and 6.0 cm (○). The solid lines correspond to a $-\frac{1}{2}$-power slope and the dashed line represents a $-\frac{1}{2}$-power slope.

strip. Finally, the paper was exposed to bright light and the developed photographic chart revealed two sharp lines separating the different exposure levels. A photograph of a short section of the photosensitive paper strip exhibiting the still-water level and wave-amplitude trace is presented in figure 4. As one can see, the end result of this measurement technique is a permanent, continuous record of wave amplitude as a function of radial position. Owing to the low surface tension of the working fluid, the liquid was observed to wet the sensitive side of the photographic paper with a contact angle of the order of 30°. Wave-amplitude measurements are obtained by

differencing the amplitude trace from the free-surface level (figure 4) under the tacit assumption that the meniscus heights of the fluid in both its static and dynamic state are nearly equal. With this supposition, the wave amplitude can be readily measured (using a suitable calibrated optical magnifying instrument) to a precision limited only by the emulsion grain size. Repeated measurements show that the amplitude error obtained for the optical scale employed in this experiment is about ± 0.1 mm, and measured values fell in the 5–17 mm range.

The reader will, of course, realize that this new measurement technique is applicable only to a single propagating free-surface wave, or to the largest-amplitude wave in a system of free-surface waves such as a solitary wave train. Thus it is particularly well suited to this experiment wherein the large-amplitude lead wave (figure 3, (*a*)) is followed by a secondary cylindrical wave (figure 3, (*b*)) formed by reflection of the initial disturbance from the corner behind the diaphragm. The smaller-amplitude trailing wave was observed to remain distinctly separated from the faster-moving primary wave.

Measurements from eight experiments, two at each of four fluid depths ranging from 4.5–6.0 cm, are presented in figure 5(*a*, *b*). Slopes corresponding to the linear $-\frac{1}{2}$ and nonlinear $-\frac{2}{3}$ wave-attenuation power laws are presented for comparison. The initial short regions of nearly constant-amplitude wave motion observed for fluid depths 5.5 cm and 6.0 cm in figure 5(*a*) are a result of transient wave formation from the piston displacement and are not relevant to the long-time evolution of interest in this study. There is some evidence from the experimental data [e.g. see figure 5(*a*), $h = 4.5$ cm and figure 5(*b*), $h = 5.5$ cm] that the lead wave passes through a linear regime before undergoing a rather abrupt transition to the nonlinear regime. This feature will be discussed in more detail in §4.

Space–time trajectories of the free-surface waves could have been obtained using a series of electronic wave gauges placed at intervals along a ray normal to the wave crest. However, we choose to test this aspect of the theory with existing internal-wave experiments (Maxworthy 1980) for which trajectory measurements are far more easily obtained. Furthermore, this permits an evaluation of results derived from the CKdV equation with respect to wave motion in a stratified fluid system.

3.2. *Cylindrical internal waves*

As part of an extensive experimental investigation on the formation of nonlinear internal waves, Maxworthy (1980, figure 13(*a*, *b*)) has presented phase trajectories for cylindrical waves evolving from gravity currents propagating radially outward into a density-stratified fluid. The density profile $\rho(z)$ was formed by emptying the contents of a container of dyed heavy salt solution under a clear thick layer of fresh water. The interface between saline and fresh water mixed and diffused into an error-function profile matching 9 cm of fresh water overlying 1 cm of salt water with density jump $\Delta\rho \approx 0.01$ g/cc. The waves were inherently visible owing to the local thickening of the lower dyed layer produced by the propagating internal wave, and position–time measurements were obtained via overhead photography. A temporal record of wave amplitude at the radial position $r_p = 205$ cm was made by monitoring the output of a density probe placed at a fixed location in the pycnocline.

To effect a comparison with Maxworthy's (1980) data, we model his measured density profiles as a two-layer fluid system for which the depth of the lower fluid layer is

$$h_1 = \frac{1}{\rho_1}\int_0^h [\rho(z) - \rho_2]\,\mathrm{d}z,$$

Fig. no.	$\Delta\rho$ (g/cc)	h_1 (cm)	c_1 (cm/s)	$(dr/dt)_0$ (cm/s)	r_0 (cm)	a_0 (cm)
6(*a*)	0.0102	0.889	2.86	5.22	110	0.81
6(*b*)	0.0104	1.063	3.06	5.62	147	0.97

TABLE 1. Calculated parameters for the two-layer-fluid model and matching-point values for the theoretical trajectories given by (8). The total fluid depth is $h = h_1 + h_2 = 9.7$ cm.

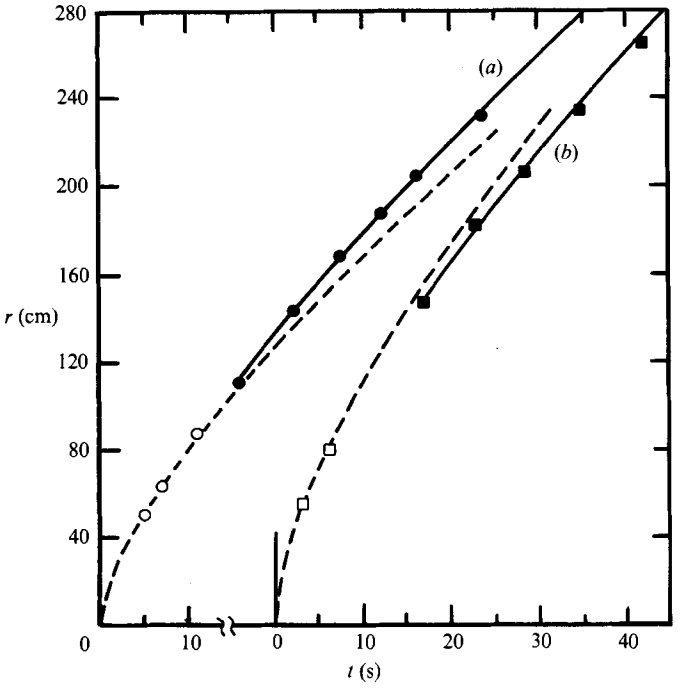

FIGURE 6. Radial internal-wave trajectories measured by Maxworthy (1980) for (*a*) small and (*b*) large initial disturbances. The dashed lines represent Maxworthy's fitted $t^{\frac{2}{3}}$ curves describing the initial stage of gravity-current trajectories. Separation of the cylindrical wave from the gravity current occurs between the open and closed symbols in each trajectory. The solid lines represent the theoretical results obtained by matching equation (8) in value and slope at the first solid point in each data set.

where $\rho_1 = \rho(0)$ and $\rho_2 = 1.00$ g/cc. The integration was performed by first curve-fitting the original data† and then numerically calculating the area under the curve using Simpson's rule. The ambient stratification parameters and the linear phase speeds determined from (10) are listed in table 1. (The fact that we have a stress-free boundary condition instead of a rigid upper boundary as assumed in Benney's (1966) analysis can be shown to have a negligible effect on the linear phase speed of these internal waves.) We are implicitly assuming that the waves in Maxworthy's experiments may be modelled as shallow-water solitary waves rather than deep-water solitary waves of the type considered by Benjamin (1967), Davis & Acrivos (1967) and Ono (1975). Inspection of Maxworthy's original photographs reveals that

† We are grateful to Professor T. Maxworthy for providing copies of all relevant experimental data and photographs necessary to make a valid theoretical comparison.

the lead cylindrical wave separated from the gravity current somewhat before $r_0 = 110$ cm for the data reported here in figure 6(*a*), and before $r_0 = 147$ cm for the more energetic case reproduced in figure 6(*b*). These radii are choosen as the reference position for comparison with the theoretical trajectories given by (8). The unknown reference amplitudes a_0 are then determined by matching experimental and theoretical velocities at $r = r_0$. The experimental wave speeds $(\mathrm{d}r/\mathrm{d}t)_0$ are determined from the slope at r_0 of a fourth-degree polynominal least-squares fit to each experimental trajectory. When the measured parameters are inserted in (9), one obtains a_0 as the solution of a cubic algebraic equation. The matching-point data are listed in table 1, and the resulting theoretical trajectories emanating from this point are drawn as solid curves in figure 6.

4. Numerical experiments on the effect of initial waveform

As previously mentioned, the experimentally determined peak amplitudes for the free-surface-wave experiments displayed in figure 5(*a*, *b*) appear in several instances to pass through short, well-defined regions of linear ($a \propto r^{-\frac{1}{2}}$) attenuation before evolving into the nonlinear ($a \propto r^{-\frac{2}{3}}$) regime. Also, for the sech-squared input profile used to generate the numerical results in figures 1 and 2 we see that the transition to the $-\frac{2}{3}$ slope occurs quite rapidly when compared to the measurements given in figure 5(*a*, *b*). In order to better understand these aspects of the measurements, we hereby present results of three parameter studies designed to investigate the effect of initial disturbance profiles on amplitude evolution described by the CKdV equation (2). Specifically, we consider (Case 1) the effect of waveform section area for solitary wave-like disturbances wherein $a\lambda^2 = \text{const.}$, (Case 2) the effect of wave steepness with constant waveform area, and (Case 3) the effect of wave skewness with constant waveform area. All numerical computations are initiated with disturbance profiles centred at $\xi = 10$. We note at the outset that all disturbances are isolated waves of elevation and in each case the disturbance volumes are sufficiently small to preclude wave fissioning, i.e. each initial waveform evolves into a single solitary wave followed by a shelf and dispersive tail. The results of the three case studies are discussed in turn below.

Case 1

We first consider the effect of changing the waveform section area for initial disturbances having the planar solitary-wave profiles

$$\zeta(10, \tau) = \alpha^2 \operatorname{sech}^2(\sqrt{\tfrac{1}{2}}\alpha\tau). \tag{11}$$

The waveform areas are equal to $4\alpha/\sqrt{3}$ and we vary the parameter α over the range $0.4 < \alpha < 1.2$. Evolution curves of the peak amplitude ζ_p are presented in figure 7. Apart from the vertical displacement of each curve with increasing α, there are only minor qualitative differences between them. In each case the evolution to the nonlinear asymptotic decay law is smooth and the radial extent for transition increases gradually with decreasing α. There are no distinct regions exhibiting purely linear $r^{-\frac{1}{2}}$ amplitude decay.

Case 2

In this numerical survey we follow the evolution of disturbances of the form

$$\zeta(10, \tau) = \alpha \operatorname{sech}^2(\sqrt{\tfrac{1}{2}}\alpha\tau) \tag{12}$$

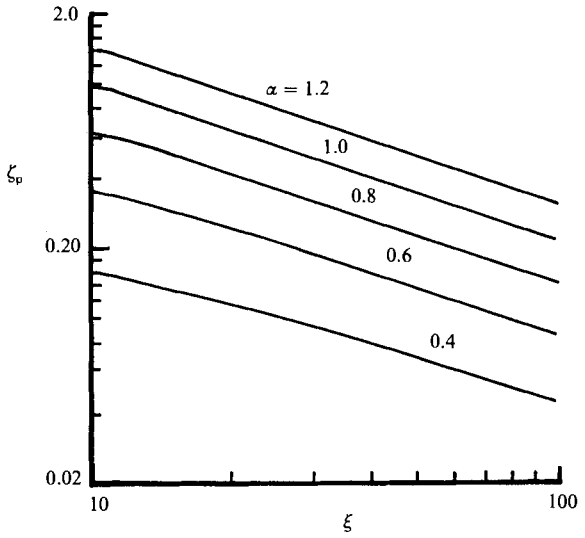

FIGURE 7. Amplitude evolution curves computed by numerical integration of equation (2) with initial sech-squared profiles given by (11).

shown plotted in figure 8(*a*) over the amplitude range $0.4 < \alpha < 1.2$. These profiles do not have the solitary-wave feature $a\lambda^2 = \text{const}$. Rather, the wave shapes are characterized by a constant-waveform-section area equal to $4/\sqrt{3}$. The evolution curves presented in figures 8(*b*) each exhibit smooth transitions to the asymptotic $r^{-\frac{2}{3}}$ attenuation law. For $\alpha = 1.2$ the initial waveform is locally too steep, and the wave profile rapidly collapses to merge into the nonlinear regime. As α decreases, the adjustment to the asymptotic state occurs over progressively longer time periods. The evolution curves for $\alpha < 0.6$ are reminiscent of the experimental measurements, suggesting that relatively low-amplitude, long-wavelength disturbances were produced by the piston displacement. Diminishing the amplitude in this case has a more profound effect on waveform evolution when compared to the previous study for solitary wave-like disturbances. In particular, one observes distinctly longer radial transition regions as the disturbance amplitude decreases. It is clear from the results in figure 8(*b*), however, that there are no well-defined regions of $r^{-\frac{1}{2}}$ behaviour, but rather the adjustment to the nonlinear regime may be characterized as a continuous, smooth transition.

Case 3

In our final study, we investigate the effect of skewness with the idea that skewed initial waveforms may precipitate distinct regions of purely linear amplitude decay. The initial waveforms for this survey are given by

$$\zeta(10,\tau) = \frac{4}{\sqrt{3}\beta(m+n)}[m\exp(-\tau/\beta - e^{-\tau/\beta}) + n\exp(\tau/\beta - e^{\tau/\beta})], \tag{13}$$

wherein the parameter β affects the wave steepness and m and n are integers in the range [0, 2] such that $m+n = 2$. The waveform area for each profile is again constant and equal to that in Case 2, namely $4/\sqrt{3}$. For $m = 2$ and $n = 0$ the waveform has positive skewness $s = 1.30$ (cf. Abramovitz & Stegun 1975). Waveforms of this type are plotted in figure 9(*a*) for $\beta = 1.5$, 2.0, and 3.0, and we note that positive skewness

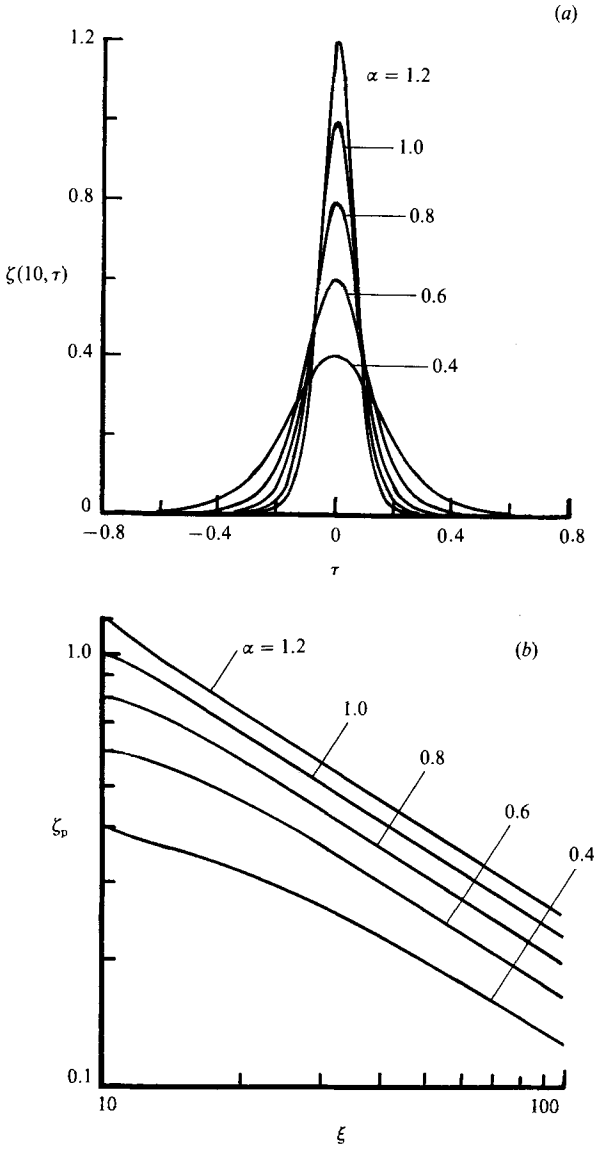

FIGURE 8. (*a*) Constant-volume profiles $\zeta(10, \tau)$ with parameter α defined by equation (12) used to test the effect of wave steepness on amplitude evolution. The volume under each curve is equal to $4/\sqrt{3}$. (*b*) Amplitude evolution curves computed by numerical integration of CKdV equation (2) using the profiles plotted in (*a*) as initial data.

corresponds to backward-tilting profiles. Forward-tilting profiles have negative skewness $s = -1.30$, and this is obtained by setting $m = 0$ and $n = 2$ in (13). Fixing $m = n = 1$ results in a symmetric profile with zero skewness.

Evolution curves for ζ_p at the three values of β, each with positive, zero, and negative skewness, are presented in figure 9(*b*). Of all the possible choices for β, we present only those that most closely mimic the experimental data. The skewness has a profound effect in that the positively skewed profiles rise in amplitude while the negatively skewed profiles fall in amplitude before merging smoothly into the nonlinear regime. While the $s = 0$ and $s = 1.30$ curves evolve with continuously

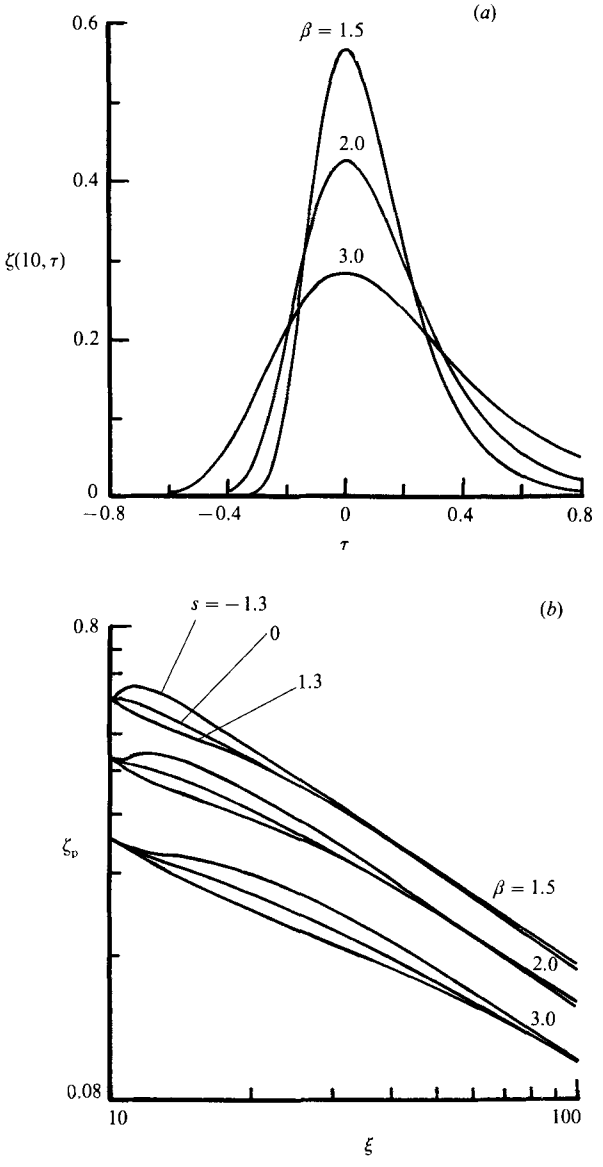

FIGURE 9. (*a*) Constant-volume profiles $\zeta(10, \tau)$ with parameter β defined by equation (13) used to test the effect of skewness on amplitude evolution. The volume under each curve is equal to $4/\sqrt{3}$. (*b*) Amplitude evolution curves computed by numerical integration of CKdV equation (2) using the profiles plotted in (*a*) as initial data.

changing slopes into the nonlinear regime, the negatively skewed disturbances do exhibit increasingly broader regions (as the parameter β increases) of nearly constant power-law attenuation before undergoing transition to the nonlinear regime. However, power-law fits of the form τ^{μ} to these regions for $s = -1.30$ show that the exponent μ varies from curve to curve, and in each case $\mu > -\frac{1}{2}$ so that no curve exhibits a discernible region of purely linear cylindrical distortion.

5. Discussion of results

Considering first the free-surface-wave experiments, it is clear that initial isolated disturbances ultimately evolve into the asymptotically predicted nonlinear Green's law, $a \propto r^{-\frac{2}{3}}$. The logarithmic correction term in (7) produces no significant contribution since these long waves have, in fact, travelled only a few wavelengths in the nonlinear regime. For the same reason, and because the diverging sidewalls had negligible effect on the wave system, no discernible influence of boundary friction is apparent. Hence these experiments tend to be far more 'ideal' than similar free-surface-wave experiments in long, narrow channels (cf. Ippen, Kulin & Raza 1955; and Weidman & Maxworthy 1978).

The numerically computed evolution curves obtained from three parameter studies on waveform shape in §4 suggest that the piston displacements did not result in solitary-wave-like disturbances. Comparison between numerical and experimental amplitude evolution curves suggests that the wave generator produced low-amplitude, symmetric or possibly negatively skewed initial waveforms. The numerical study showed no evidence of distinct $r^{-\frac{1}{2}}$ amplitude decay prior to the nonlinear regime. On the other hand, as pointed out in §3.1, several of the measured evolution curves do exhibit this trend. We can only conclude that the relatively well-defined transition between $r^{-\frac{1}{2}}$ and $r^{-\frac{2}{3}}$ power laws observed in certain examples of the experimental data is not supported by integrations of the CKdV equation for initial waveforms considered here. Perhaps an inclusion of higher-order cylindrical dispersion terms, similar to the analysis of Chwang & Wu (1976), is necessary to capture this observed feature.

Turning now to the internal-wave trajectories in figure 6, we again note that the logarithmic correction term in the analytical solution of Ko & Kuehl (1978) does not affect the phase trajectories owing to the small value of the k-coefficient in (8), and the limited extent of wave propagation beyond the radial matching points r_0. Bottom friction may be important for these waves since they scale with the lower fluid depth h_1, and therefore propagate many more wavelengths across the tank in comparison to the free-surface waves. However, wave dissipation is not evident in the comparison between experimental and theoretical trajectories in figure 6, unless one infers that the experimental data for the most energetic case in figure 6(b) are beginning to lag behind the theoretical trajectory. It is not surprising that the phase-trajectory comparisons based on the two-layer approximation work so well in this case. Previous calculations by Weidman & Johnson (1982) indicate that linear phase speeds for internal waves propagating along a pycnocline are accurately predicted using broken-line models for the measured density profiles.

A comparison of theoretically inferred amplitudes with Maxworthy's (1980) measurements can also be made. Calculating the wave amplitudes at the probe radius $r_p = 205$ cm, we find from (7) the theoretical values $a_p = 0.53$ cm and 0.79 cm, to be compared with the measured values $a_p = 0.35$ cm and 0.90 cm, respectively. There are two important considerations in making this comparison. First, the amplitude measurements depend on the vertical location of the conductivity probe within the pycnocline and hence cannot be directly compared to the theoretical value for a two-layer system. Second, and perhaps more importantly, this comparison tacitly assumes 'weak nonlinearity' when in fact the smallness parameter, evaluated at the matching points listed in table 1, is about $a_0/h_1 = 0.9$. Concerning this latter point, Maxworthy's original photographs indicate that the waves in the neighbourhood of

r_0 still contained coloured dye from the gravity-current intrusion. This implies closed streamlines within the cylindrical wave, a clear manifestation of strong nonlinear effects.

6. Conclusion

In summary, we have made direct comparisons between theory and experiment on the evolution of nonlinear cylindrical waves propagating in both homogeneous and stratified fluid ambients. New experiments using a novel 'highest-amplitude' measurement technique clearly exhibit the predicted $r^{-\frac{2}{3}}$ power-law decay for these weakly nonlinear waves. It is pointed out that the cylindrical Korteweg–de Vries equation derived by Miles (1978) in the context of free-surface gravity waves also applies to internal gravity waves propagating in a density-stratified fluid. Direct comparison of predicted phase trajectories with internal-wave measurements reported by Maxworthy (1980) is effected by modelling his continuous pycnocline as a layered two-fluid system. The good corroboration between theoretical and experimental space–time trajectories is indicative of the low energy loss due to viscous dissipation in these axisymmetric, laboratory-scale wave systems.

A numerical study of the effects of initial disturbance waveform on the amplitude evolution of cylindrical waves has been performed to interpret certain aspects of the free-surface wave experiments. Parameters varied include waveform area, wave steepness, and wave skewness. The results suggest that although the amplitude history is markedly affected by wave steepness and skewness, the evolving waveforms exhibit no distinct region of purely linear radial distortion preceeding the nonlinear regime. Rather, the numerical study based on the CKdV equation exhibits continuous, smooth transitions of disturbance waveforms to slowly varying cylindrical solitary waves.

We are grateful to T. Maxworthy for use of his experimental facility in which these measurements were conducted and for financial support under an ONR contract to the University of Southern California. Casey de Vries provided expert technical assistance. Helpful discussions with N. Pereira and L. Redekopp on the subject of this paper are also acknowledged and we extend our thanks to K. Ko for guidance in development of the numerical code. The comments of two referees provided valuable improvement for the final manuscript. This work was partially supported by ONR Grant No. N00014-86K-0728.

REFERENCES

Abramovitz, M. & Stegun, I. A. 1975 *Handbook of Mathematical Functions.* Dover.

Benjamin, T. B. 1967 Internal waves of permanent form in fluids of great depth. *J. Fluid Mech.* **29**, 559.

Benney, D. J. 1966 Long nonlinear waves in fluid flows. *J. Math. Phys.* **45**, 52.

Calogero, F. & Degasperis, A. 1978 Solution by the spectral-transform method of a nonlinear evolution equation including as a special case the cylindrical KdV equation. *Lett. Nuovo Cim.* **23**, 150.

Chang, P., Melville, W. K. & Miles, J. W. 1979 On the evolution of a solitary wave in a gradually varying channel. *J. Fluid Mech.* **95**, 401.

Chwang, A. T. & Wu, T. Y. 1976 Cylindrical solitary waves. *Proc. IUTAM Symp. on Water Waves in Water of Varying Depth, Canberra, Australia.*

CUMBERBATCH, E. 1978 Spike solution for radially symmetric solitary waves. *Phys. Fluids* **21**, 374.

DAVIS, R. E. & ACRIVOS, A. 1967 Solitary internal waves in deep water. *J. Fluid Mech.* **29**, 593.

GRIMSHAW, R. 1979 Slowly varying solitary waves. I. Korteweg–de Vries equation. *Proc. R. Soc. Lond.* A **368**, 359.

HAMMACK, J. L. & SEGUR, H. 1974 The Korteweg–de Vries equation and water waves. Part 2. Comparison with experiments. *J. Fluid Mech.* **65**, 625.

IPPEN, A. T., KULIN, G. & RAZA, M. A. 1955 Damping characteristics of the solitary wave. *Hydrodyn. Lab., M.I.T. Tech. Rep.* 16.

JOHNSON, R. S. 1973 On an asymptotic solution of the Korteweg–de Vries equation with slowly varying coefficients. *J. Fluid Mech.* **60**, 813.

KAKUTANI, T. 1971 Effect of an uneven bottom on gravity waves. *J. Phys. Soc. Japan* **30**, 272.

KAUP, D. J. & NEWELL, A. C. 1978 Solitons as particles, oscillators, and in slowly changing media: a singular perturbation theory. *Proc. Roy. Soc. Lond.* A **361**, 413.

KO, K. 1978 Korteweg–de Vries soliton in a slowly varying medium. PhD thesis, University of Southern California.

KO, K. & KUEHL, H. H. 1978 Korteweg–de Vries soliton in a slowly varying medium. *Phys. Rev. Lett.* **40**, 233.

KO, K. & KUEHL, H. H. 1979 Cylindrical and spherical Korteweg–de Vries solitary waves. *Phys. Fluids* **22**, 1343.

LEIBOVICH, S. & RANDALL, J. D. 1973 Amplification and decay of long nonlinear waves. *J. Fluid Mech.* **53**, 481.

MAXON, S. & VIECELLI, J. 1974 Cylindrical solitons. *Phys. Fluids* **17**, 1614.

MAXWORTHY, T. 1980 On the formation of nonlinear internal waves from the gravitation collapse of mixed regions in two and three dimensions. *J. Fluid Mech.* **96**, 47.

MILES, J. W. 1977 Note on a solitary wave in a slowly varying channel. *J. Fluid Mech.* **80**, 149.

MILES, J. W. 1978 An axisymmetric Boussinesq wave. *J. Fluid Mech.* **84**, 181.

ONO, H. 1975 Algebraic solitary waves in stratified fluids. *J. Phys. Soc. Japan* **39**, 1082.

OSTROVSKIY, L. A. & PELINOVSKIY, E. N. 1975 Refraction of nonlinear sea waves in a coastal zone. *Izv. Acad. Nauk SSSR, Atmos. Ocean. Phys.* **11**, 37.

PERROUD, P. H. 1957 The solitary reflection along a straight vertical wall at oblique incidence. PhD thesis, University of California, Berkeley.

SHUTO, N. 1974 Nonlinear waves in a channel of variable section. *Coastal Engng Japan* **17**, 1.

SU, C. H. & MIRIE, R. M. 1980 On head-on collisions between two solitary waves. *J. Fluid Mech.* **98**, 509.

VLIEGENTHART, A. C. 1971 On finite difference methods for the KdV equation. *J. Engng Maths* **5**, 2.

WEIDMAN, P. D. & JOHNSON, M. 1982 Experiments on leapfrogging internal solitary waves. *J. Fluid Mech.* **122**, 195.

WEIDMAN, P. D. & MAXWORTHY, T. 1978 Experiments on strong interactions between solitary waves. *J. Fluid Mech.* **85**, 417.